PROCEEDINGS OF SCIENCE

Large-scale extraplanar PAH emission in the Galactic center region found by AKARI mid-infrared all-sky survey

T. Kondo[*,a] **H. Kaneda,**[a] **D. Ishihara,**[a] **S. Oyabu,**[a] **M. Yamagishi**[a] **and T. Onaka**[b]
[a]*Graduate School of Science, Nagoya University, Chikusa-ku, Nagoya 464-8602, Japan*
[b]*Graduate School of Science, The University of Tokyo, Bunkyo-ku, Tokyo 113-0033, Japan*
E-mail: kondo@u.phys.nagoya-u.ac.jp

AKARI carried out all-sky surveys at wavelengths of 9, 18, 65, 90, 140 and 160 μm. Among them, the 9 μm map can efficiently trace the emission features of polycyclic aromatic hydrocarbons (PAHs). Utilizing this unique all-sky PAH map, we investigate the distribution of the PAH emission for the whole Galactic plane. In particular, the Galactic center regions suffer foreground contamination by the zodiacal light, and therefore we have carefully removed the zodiacal light component by modifying the Kelsall model. As a result, we find that the PAH emission is extended very widely ($\sim 30^{\circ}$) toward the north direction from the Galactic center region. Since it is known that there are very nearby ($\sim$150 pc) Ophiuchus clouds toward similar directions, we subtracted the foreground component associated with these clouds using the HI data. As a result, we confirm that there still remains a significant fraction of the widely-extended PAH emission toward this direction, suggesting that the excess PAH emission originates in the Galactic center region. The spatial distribution resembles that of the Fermi bubbles, well-known gamma-ray structures, which are thought to be created by a past outflow in the Galactic center. Moreover, the PAH/dust ratio is significantly enhanced in the region showing the excess PAH emission. The high PAH/dust ratio is possibly created by shattering of carbonaceous grains in the past outflow from the Galactic center.

The Life Cycle of Dust in the Universe: Observations, Theory, and Laboratory Experiments - LCDU 2013, 18-22 November 2013
Taipei, Taiwan

[*]Speaker.

PoS(LCDU 2013)033

1. Introduction

Polycyclic aromatic hydrocarbons (PAHs) are ubiquitous in the general interstellar medium in our Galaxy and nearby galaxies (e.g., [1], [2], [3]). They show good spatial correlations with HI, molecular gas, and dust grains emitting far-infrared (far-IR) emission [4]. AKARI has great advantages in observing PAHs on various spatial scales. AKARI carried out all-sky surveys in the 9, 18, 65, 90, 140 and 160 μm bands. Among them, the 9 μm all-sky survey can efficiently trace the PAH emission features, as compared with the IRAS and WISE 12 μm band observations. In consequence, we obtain the all-sky PAH map with spatial resolution of $\sim 6''$, which is higher than the IRAS 12 μm map by one order of magnitude. Using this map, we investigate the distribution of the PAH emission for the whole Galactic plane.

2. Production of the all-sky PAH map

Figure 1 (a) shows the 9 μm all-sky map in galactic coordinates. There is a bright emission component along the ecliptic plane, in addition to the Galactic plane emission. This is the zodiacal light, the thermal emission from the interplanetary dust (IPD) in our Solar System. The zodiacal light is a dominant foreground component in the mid-IR, and therefore we need to remove the zodiacal light accurately in order to study the diffuse Galactic emission.

2.1 The zodiacal light model

The zodiacal light has been studied with past IR surveys and many efforts have been made to model it. Kelsall et al. [5] built the zodiacal light model based on the COBE/DIRBE observations (hereafter the Kelsall model). In this model, the zodiacal light is divided into three components: a smooth cloud, asteroidal dust bands, and the resonance component trapped by the Earth into resonant orbits near 1 AU. For each of the three components, Kelsall et al. introduced parameterized functions describing the spatial distribution of the dust number density in heliocentric coordinates (X,Y,Z). They estimated the intensity of the zodiacal light at wavelength λ for each pixel p at time t as an integral along the line of sight of the thermal emission, summed over each component c:

$$Z_\lambda(p,t) = \sum_c \int n_c(X,Y,Z)\varepsilon_{c,\lambda}B_\lambda(T)ds, \tag{2.1}$$

where $n_c(X,Y,Z)$ is the density for each of the components, $\varepsilon_{c,\lambda}$ is the emissivity for component c at wavelength λ.

2.2 Modification of the zodiacal light model

For the estimation of the zodiacal light intensity, Kelsall et al. utilized seasonal variations of the zodiacal light in order to separate the zodiacal light component from the Galactic component. They compared the variations between the observations and the model predictions, and optimized geometrical parameters and the emissivities. As a result, they were able to remove the zodiacal light from the DIRBE maps, whose residual component level is $\sim 8\%$ of the intensity of the original zodiacal light around the ecliptic plane. In the same manner, we tried removing the zodiacal light from the AKARI 9 μm map and obtained the result shown in Figures 1 (b) and (with enhanced

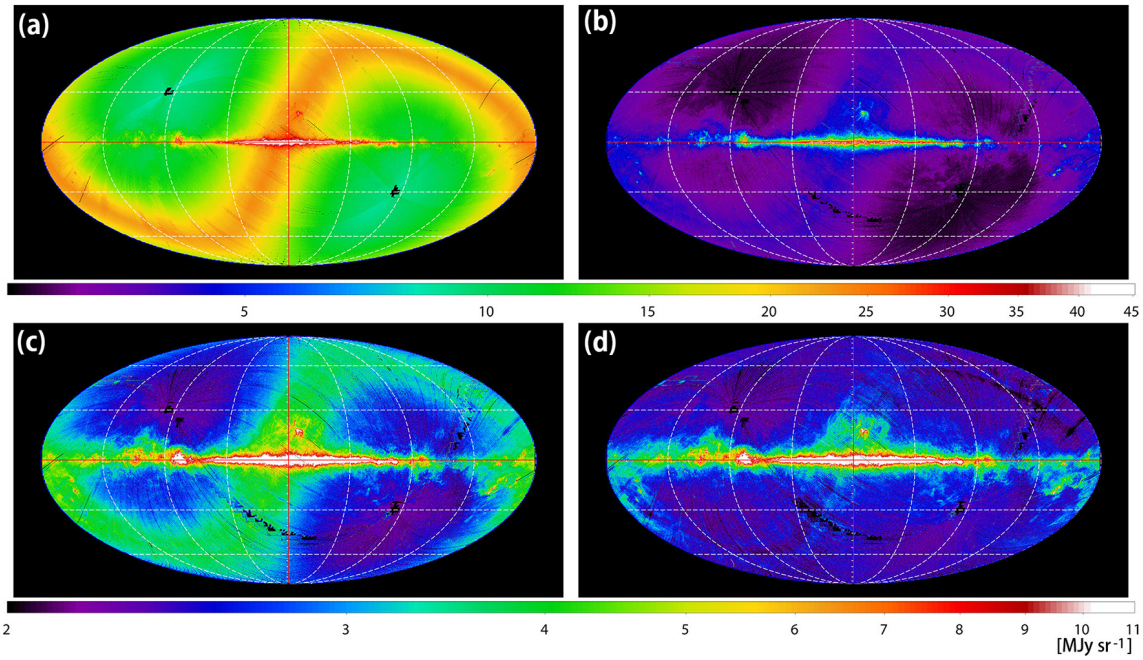

Figure 1: AKARI 9 μm all-sky maps in galactic coordinates. (a) The map before the zodiacal light is removed. (b) The map after the zodiacal light is removed with the Kelsall model. The color scale is the same as panel (a). (c) The same map as panel (b) but the color scale is adjusted to emphasize the residual component. (d) The map after the zodiacal light is removed in our new method. The color scale is the same as panel (c).

color contrast) (c). As can be seen in Figure 1 (c), there is still residual emission remaining after the traditional method of removing the zodiacal light, such that any extended diffuse Galactic component, especially near the Galactic center, cannot be disentangled from this.

Thus, we try to improve the accuracy by modifying the Kelsall model. We specifically optimize the model parameters using not only the seasonal variations but all the seasonal raw data after masking the Galactic plane (regions of $\geq$7 MJy sr^{-1} in the IRAS 100 μm map). As a result, the model parameters are changed from those in the previous study. For example, the density of the resonance component becomes twice as large as the previous result and the center position of the IPD cloud is significantly changed. The result of the zodiacal light subtraction is apparently improved as shown in Figure 1 (d), the residual component level is only about 1 to 2% of the intensity of the original zodiacal light. This result suggests that the zodiacal light is composed of time-varying and static components, and we successfully reproduce both components by modifying the model parameters.

3. Extraplanar PAH emission in the Galactic center region

Using our processed 9 μm PAH map, we study the PAH emission on various spatial scales: from local to global scales. In this paper, we discuss large-scale structures in the Galactic center region. Figure 2 (a) shows the AKARI 9 μm map of approximately $100^\circ \times 90^\circ$ around the Galactic center region. As can be seen in the figure, PAH emission is widely extended toward the north.

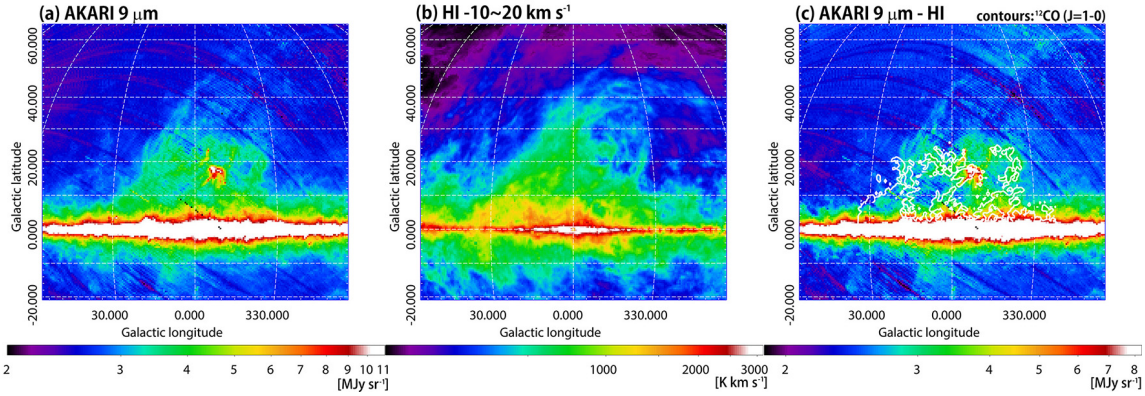

Figure 2: Maps of approximately $100^\circ \times 90^\circ$ around the Galactic center region. (a) The AKARI 9 μm map. (b) The Leiden/Argentine/Bonn Galactic HI survey map integrated over the velocity range of $-10 \sim +20$ km s^{-1}. (c) The 9 μm map after subtracting the PAH component associated with nearby foreground clouds using the HI data. The contours indicate the NANTEN ^{12}CO (J =1–0) integrated intensity. The contour level is 1.4 K km s^{-1}.

The nearby ($\sim$150 pc) Ophiuchus and Lupus cloud complexes are located in the same line of sight in this region (e.g., [6]). Figure 2 (b) shows the HI map in the velocity range corresponding to the clouds ($V_{\rm LSR} = -10 \sim +20$ km s^{-1}; [6]), which is obtained from the Leiden/Argentine/Bonn Galactic HI survey. Assuming a tight correlation between the distributions of PAHs and HI gas, we subtract the PAH component associated with the nearby clouds by scaling the HI data. The scale factor is estimated from the intensity ratios of the 9 μm emission over the HI emission in the surrounding regions. The result is shown in Figure 2 (c), where we confirm that there still remains a significant fraction of widely-extended PAH emission to the north of the Galactic center. The contours overlaid on this figure indicate the distribution of nearby molecular clouds obtained by the ^{12}CO (J =1–0) observations with the NATEN radio telescope. As shown in this figure, most of the extended residual PAH component is not associated with the clumpy CO molecular clouds. More than 70% of the areas where the signal-to-noise ratios of the PAH emission are higher than five are not covered by the CO emission. From the above, the residual component is not likely to be associated with the nearby foreground clouds, and thus possibly associated with the Galactic center.

Next, we compare the spatial distributions of the residual PAH component with the Fermi gamma-ray bubbles revealed by subtracting the Galactic foreground emission from the all-sky gamma-ray map obtained by the Fermi Gamma-ray Space Telescope [7]. The Fermi bubbles exhibit extended bipolar structures as shown in Figure 3 and they are considered to be associated with a past outflow in the Galactic center (the area surrounded by a white frame in Figure 3 is the same area as in Figure 2). Comparing the residual PAH component (Figure 2 (c)) with the Fermi bubbles (Figure 3), both structures seem to be similar in distribution near the Galactic center. This result also suggests the possibility that the residual PAH component originates in the Galactic center.

In order to investigate the properties of the residual PAH component, we compare the distribution of PAHs with that of dust grains. For this comparison, we calculate the integrated intensities of the PAH emission and the far-IR emission from dust grains which have typical temperature in the

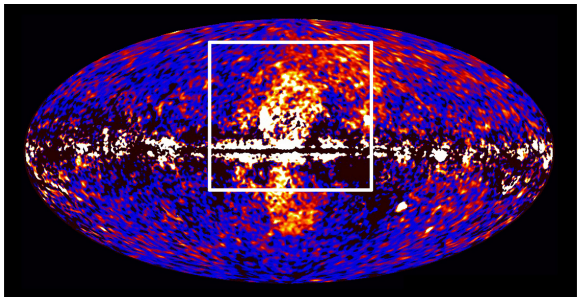

Figure 3: Fermi bubbles discovered by the processed Fermi all-sky data at energies of 1–10 GeV. The white frame corresponds to the area shown in Figures 2 and 4. **Credit:** NASA/DOE/Fermi LAT/D. Finkbeiner et al.

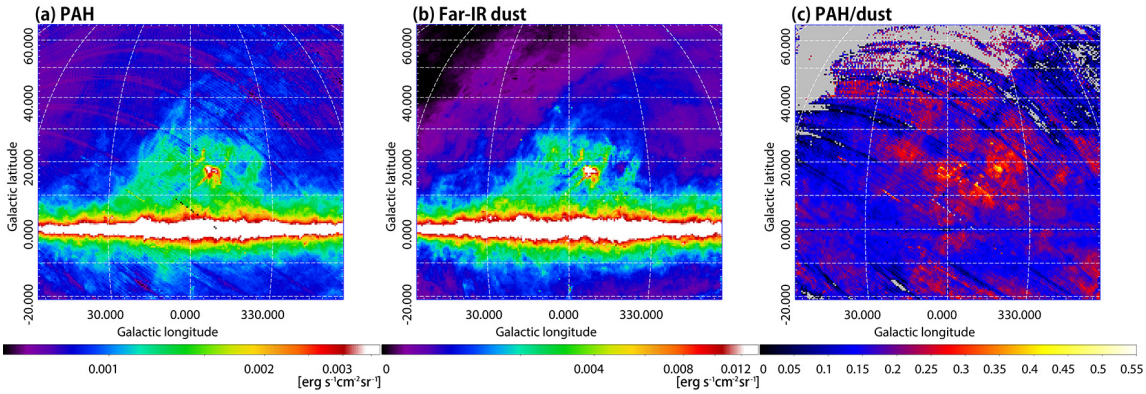

Figure 4: (a) Integrated intensity map of the PAH emission. (b) Integrated intensity map of the far-IR dust emission. (c) Distribution of the ratio of the PAH to the dust integrated intensity. The areas where signal-to-noise ratios are lower than five in the PAH or the dust emission map are masked.

interstellar radiation field using the AKARI 9 μm and the AKARI 65, 90 and 140 μm all-sky data, respectively. Figures 4 (a) and (b) show the distributions of the PAH and dust emission, respectively. They show spatial distributions similar to each other, reflecting that PAHs and dust grains are mixed well in interstellar space (e.g., [1], [8]). Yet, there are regional variations in the intensity ratio of PAH to dust, as can be seen in Figure 4 (c). We find that the PAH/dust ratio is high in the region where the residual PAH component is relatively strong. From the similarity in distributions between the PAH/dust ratio (Figure 4 (c)) with the Fermi bubbles (Figure 3), we suggest here that the PAH/dust ratio may be related to the Fermi bubbles. The overabundance of PAHs can be explained by shattering of larger carbonaceous grains in these outflows (e.g., [9]).

4. Summary

The AKARI 9 μm all-sky map efficiently traces the emission features of PAHs. In order to utilize this unique all-sky PAH map, we have carefully removed the zodiacal light by modifying the Kelsall model. We have succeeded in reducing the residual component level to $\sim$1–2% of the intensity of the original zodiacal light. Using the 9 μm PAH map thus processed, we find large-scale excess PAH emission near the Galactic center, the spatial distribution of which resembles

that of the Fermi bubbles. Moreover, the PAH/dust ratio is significantly enhanced in the region showing the excess PAH emission. The high PAH/dust ratio is possibly created by shattering of carbonaceous grains in past outflows.

Acknowledgments

We thank all the members of the AKARI project. T.K. is financially supported by Grants-in-Aid for JSPS Fellows No. 25-2536.

References

[1] T. Onaka, et al., *Detection of the Mid-Infrared Unidentified Bands in the Diffuse Galactic Emission by IRTS, PASJ* **48**, L59 (1996)

[2] J. D. T. Smith, et al., *The Mid-Infrared Spectrum of Star-forming Galaxies: Global Properties of Polycyclic Aromatic Hydrocarbon Emission, ApJ* **656**, 770 (2007) [astro-ph/0610913]

[3] H. Kaneda, et al., *Properties of Polycyclic Aromatic Hydrocarbons in Local Elliptical Galaxies Revealed by the Infrared Spectrograph on Spitzer, ApJ* **684**, 270 (2008) [astro-ph/0805.3257]

[4] G. J. Bendo, et al., *The relations among 8, 24 and 160 μm dust emission within nearby spiral galaxies, MNRAS* **389**, 629 (2008) [astro-ph/0806.2758]

[5] T. Kelsall, et al., *The COBE Diffuse Infrared Background Experiment Search for the Cosmic Infrared Background. II. Model of the Interplanetary Dust Cloud, ApJ* **508**, 44 (1998) [astro-ph/9806250]

[6] K. Tachihara, et al., *^{12}CO Molecular Cloud Survey and Global Star Formation in Lupus, PASJ* **53**, 1081 (2001)

[7] M. Su, T. R. Slatyer, & D. P. Finkbeiner, *Giant Gamma-ray Bubbles from Fermi-LAT: Active Galactic Nucleus Activity or Bipolar Galactic Wind?, ApJ* **724**, 1044 (2010) [astro-ph/1005.5480]

[8] H. Kaneda, et al., *Processing of Polycyclic Aromatic Hydrocarbons in Molecular-Loop Regions near the Galactic Center Revealed by AKARI, PASJ* **64**, 25 (2012) [astro-ph/1110.2165]

[9] A. P. Jones, A. G. G. M. Tielens, & D. J. Hollenbach, *Grain Shattering in Shocks: The Interstellar Grain Size Distribution, ApJ* **496**, 740 (1996)